Journal of the Nigerian Association of Mathematical Physics
Volume33,(January, 2016), **pp139 – 146**

The Radiative Recombination Rate for Strained InAs/GaAsQuantum Dot (QD)

[1]Onyeaju M. C., [2]Idiodi J.O.A., [3]Omehe N.N. and Aghemenloh, E.

[1]Department of Physics, University of Port Harcourt, Port HarcourtRiversState
[2]Department of Physics, University of Benin, BeninCityEdoState
[3]Department of Physics, FederalUniversity, Otuoke, BayelsaState.

Abstract

Low dimensional heterostructure of InAs/GaAs Quantum dot (QD) grown epitaxially are often marked with misfit due to lattice misalignment. As a result they have longer radiative recombination time and small exciton oscillator strength. With this however, the dot is strongly confined and more charge will be trapped within the QD system. Also the quantum efficiency will be reduced and the band alignment driven by Γ-X transition with longer radiative recombination rate has been a difficult task to achieve experimentally. This is due to the small size and low density of InAs/GaAs system at nanoscale.

In view of this, mutiband envelop functional method was used for the computation of the band structure for strained InAs QD and the values obtained shows good correlation with experiments. The results of the band structure are applied to the radiative recombination rate for strained InAs/GaAs QD and a remarkable improvement was observed with those studied on literature. Also larger blue shifts were observed (14, 21, 22 and 34 meV) at the QD related peak due to a weak type II transitions observed, and i.e. electrons in the dots recombine with the holes in the barriers.

Keywords: Quantum dots; Exciton; Intersubbands; Band alignment

1.0 Introduction

Progress made in the fabrications of low dimensional heterostructure has open up many possibilities for optoelectronics devices from quantum structures. Researchers on this field have made several effort focused on the Physics of semiconductor quantum dots (QDs) [1- 3]. Self organised QDs of InAs with low densities are often marked with misfit due to lattice misalignment and are probably the best realization of the intermediate band solar cell (IBSC)[4-6] due to the prediction of zero band offset for one of the carrier types at the QD/barrier heterojunction. Self assembled QD in InAs/GaAs structures are usually characterized by relatively small size which is comparable to the exciton Bohr radius. As a consequence, they have a rather long radiative recombination time of about 1 ns and small exciton oscillator strength [5]. With such single QD excitons the strong coupling regime can be realized.

Many groups have studied the electronic structure of QDs that governs other transport and spectral properties like the optical properties [4, 7-10] that are fundamental in device applications. Recently the effects of strain and the coupling on the electronic structure of QDs where elastic fields are highly nonuniform has been widely studied [11-16] but up till now little or no attention has been paid to the effect of this strain on the core and barrier material band structures. This modifies the energy band gaps and lifts up the heavy-hole degeneracy at the zone centre. This was ignored in recent studies of the optical properties of QD confined in various shapes [8-10]

The elastic strain field has been discussed by Zhang et al.[11] and accordingly, this modifies the basic band structureparameters in semiconductor materials; for example, dilatational strain modifies the band gap while the axial and shear components of strain break the crystalline symmetry which lifts the energy degeneracy of the heavy-hole and light-hole valence subbands [11].

The electrons confined in QDs are strongly coupled to the longitudinal optical vibrations of the underlying semiconductor lattice, which leads to the formation of the so-called electronic QD polarons which are the true excitations of a charged dot.

Corresponding author: Onyeaju, M. C., E-mail:Michael.onyeaju@uniport.edu.ng, Tel.: +2348068118468

The coupling of electron/hole pairs with optical phonons, and their consequences on the optical response of semiconductor QDs have been corroborated in the study made by Ferreira et al.[17] when they studied the optical properties of excitonic polarons in semiconductor QDs. However the relaxation mechanism for polarons is still a subject of interest because of the existence of a finite-energy window for their relaxation.

Also, optical experiments have unambiguously demonstrated the couplings between confined electron/hole pairs and optical phonons [17]. The phonon bottleneck and the energy relaxation mechanism for low dimensional QD has been a subject of interest [17, 19-21] and is yet to be fully understood. Measurement by a number of groups failed to observe the bottleneck effect [17, 18-23].

The experimental signatures of the excitonic polarons state are still missing probably due to the following two reasons:

1. The electronic polarons were observed in magneto-absorption experiments, where an external parameter was used to monitor the inter-level transitions and thus allowed to induce a phonon resonance between different confined levels. However the phonon induced coupling was not large enough to be resolved spectroscopically especially in low dimensional QD system.
2. The inherent inhomogeneous broadening of the interband transitions for a dot ensemble that displays narrow features, despite the unavoidable statistical distribution of the dot size, while interband transitions are very sensitive to size dispersion [8]

Also, the band alignment for this group of QD is yet to be understood. However, the recombination rate between the electrons and holes in such a system pose a serious challenge as a result of the carrier relaxation in QDs [5, 18-23]

The purpose of this present work is to carry outtheoretical investigation on the radiative recombination rate for self-organised InAs/GaAs QD whose shape and size coicide with those extracted from experiments. Here we focus our attention on the dependance of the ground state confinrment energy, wetting layer as well as the diameter of the confining potentials. A multiband envelop functional method were employed for our numerical analysis and the result shows an improvement over that presented by Pancholi et al. [5]

2.0 Theoretical Framework/Numerical Methods

Here we look at the single band toy model of Zhang et al. [11], and construct similar model that will assume the anisotropy nature of the bands. We assume that not only does the strain induce potential play a major role in the deformation potential but also the radial spherical potential. This we have done by considering the motion of an electron in a spherical QD confined by a radial potential of the form $^1/_2\, m^*\omega_o^2 r^2$(where m^* is the effective mass of the electron, r is the position and $\omega_o$is the frequency of the QD's confinement potential)to be

$$\left[E_c - {}^1/_2\, m^*(p - {}^e/_c\, A)^2\right]\Psi(r) + {}^1/_2\, m^*\omega_o^2 r^2\Psi(r) = E\Psi(r) \qquad (1)$$

where $E_c = E^0_{c,v} + a_c r C_h$, is the energy of the conduction-band state [15], $E^0_{c,v}$ is the energy of the band edge for conduction or valence band minimum and C_h is the hydrostatic strain, p is the momentum, A is the vector potential of the magnetic field ($\vec{B}$=∇x$\vec{A}$), in the symmetric gauge $A = \left(A_p = A_z = 0,\ A_\varphi = \frac{\vec{B}X\vec{r}}{2}\right)$, r is the position and a_c is the so-called deformation potential constant which determines the extent to which mechanical strain modifies the electronic structureof the QD e.g the optical properties [11,15,24].

Thecauchy strainη is the symmetric part of the displacement gradient,

$$\eta = {}^1/_2\,(\nabla U + \nabla^T U). \qquad (2)$$

Here,

U =The strain energy density for linear elastic deformation and

$\nabla^T U$ = is the local strain tensor.

Dilatational strain in the QD is relatively constant, so that the potential is that due to the radial spherical coordinate and that of the deformation potential.

The strain tensor components are obtained by minimizing the elastic energy

$$E = \tfrac{1}{2}\int_v\ C_{ijkl}\epsilon_{ij}\epsilon_{kl}\, dv \qquad (3)$$

where $C_{ijkl}$is the fourth-ranked elastic stiffness tensor.

The piezoelectric polarization is a consequence of strain. In zinc blende materials, this polarization with respect to the crystal coordinate systemis given by

$$P^{pz}(x) = e_{14}\begin{pmatrix} 2\epsilon_{yz} \\ 2\epsilon_{xz} \\ 2\epsilon_{xy} \end{pmatrix} \qquad (4)$$

where e_{14} is the piezoelectric constant. The spatial variation of P^{pz} leads to piezoelectric charges and the resulting piezoelectric field is obtained by solving the Poisson equation

$$\nabla.\left[\varepsilon_0\varepsilon(x)\nabla\varphi(x)\right]=-\rho(x,\varphi) \quad (5)$$

where "$\varepsilon_0\varepsilon$" is the dielectric constant at position *x*, ε_0 is the permittivity of vacuum and ε is the relative permittivity of either the electrolyte or any of the semiconductor materials.$\varphi(x)$ is the electrostatic potential and $\rho(x,\varphi)$ is the charge density inside the material.

From equation (1), we obtain

$$\nabla^2\Psi+\frac{2m^*}{\hbar^2}\left(E_c-E+\frac{m^*\omega_o^2r^2}{2}-\frac{(\vec{B}X\vec{r})^2e^2}{8m^*c^2}+\frac{(\vec{B}X\vec{r})eL_z}{2m^*c}\right)\Psi=0 \quad (6)$$

where L_z is the z-component of the angular momentum operator along the growth direction (Z). The motion in the magnetic field is characterized by the cyclotron radius$r_c=\left(\frac{\hbar c}{e\boldsymbol{B}}\right)^{1/2}$, which is small for large magnetic fields.

The laplacian operator in spherical coordinate is

$$\nabla^2=\frac{1}{r^2}\frac{\partial}{\partial r}\left(r^2\frac{\partial}{\partial r}\right)+\frac{1}{r^2Sin\theta}\frac{\partial}{\partial\theta}\left(Sin\theta\frac{\partial}{\partial\theta}\right)+\frac{1}{r^2Sin^2\theta}\frac{\partial^2}{\partial\emptyset^2} \quad (7)$$

The typical practice is to transform equation (6) into an envelope functional method where the plane wave will replace the periodicity of the crystal [11, 26-28]

$$\Psi_{(r)}=\sum_{n=1}^{N_b}\left(\sum_k b_n(k)e^{ik.hr}\right)\emptyset_{n,k=0}(r) \quad (8)$$

where the term $\sum_k b_n(k)e^{ik.hr}$ is the envelope function, N_b is the number of bands, and $\emptyset_{n,k=0}(r)$ is the Bloch wave function at K= 0.

The Hamiltonian in equation (6) can be written as [11]

$$\sum_{\boldsymbol{m}}\left(\mathrm{H_{nm}(r)}+\mathrm{W_{nm}(r)F_m(r)}\right)=\mathrm{EF_n} \quad (9)$$

where $\mathrm{F_m}$ represents the envelope function and the sum may include conduction and valence bands. $W_{nm}$is the potential due to strain. The positions of the quantum size levels were calculated in spherical model together with the warping of the valence band connected with the cubic symmetry of the zinc blende lattice structure.

In the framework of the 'model solid theory' and the eight-band K·p theory, strain-modified confinement potential is given by [26].

$$E_{c,E}=E^o_{v,av}+\frac{\Delta_o}{3}+E_g+a_c\in_{hyd} \quad (10)$$

$$E_v^{hh}=E^o_{v,av}+\frac{\Delta_o}{3}+a_v\in_{hyd}-\frac{1}{2}b\in_{bi} \quad (11a)$$

$$E_v^{lh}=E^o_{v,av}-\frac{\Delta_o}{6}+a_v\in_{hyd}+\frac{1}{4}b\in_{bi}+\frac{1}{2}\sqrt{\left(\Delta_o^2+\Delta_o b\in_{bi}+\frac{9}{4}(b\in_{bi})^2\right)} \quad (11b)$$

where $E_{c,E}$ is the strain modified conduction band edge, $E^o_{v,av}$ is the unstrained average valence band-edge, Δ_o is the spin orbit splitting, $E_g$is the unstrained band gap, E_v^{hh} and E_v^{lh} are heavy and light-hole energy bands, respectively, a_c is the deformation potential for conduction band and a_v and b are valence band and shear deformation potentials, respectively. The band edge energies at Brillouin zone centre (k=0) will be estimated via equations (10-11) above.

2.1 Strain Distribution on the Dots.

We choose the reference state of a uniform undeformed substrate crystal lattice for the measurement of strains. Relative difference between lattice constants of the substrate a_s and the film a_f is the so-called "mismatch strain" given by

$$\in_0=\frac{a_s-a_f}{a_f} \quad (12)$$

and it is usually negative (compression), as $a_f>a_s$. During the film deposition, its crystal lattice is deformed to fit the crystal lattice of the substrate.

Both the film and the substrate are supposed to be isotropic linear elastic materials with the same elastic constants (which is reasonable e.g. for Ge/Si and InAs/GaAs systems) and obey usual Hooke's law [15]

$$\in_{ij}=\frac{1+v}{E}\delta_{ij}-\frac{v}{E}\delta_{kk}\delta_{ij} \quad (13)$$

where$\in_{ij},\delta_{ij},E,v$ are strain tensor, Stress, Young modulus and Poisson's ratio respectively.

For a zinc-blende type cubic crystalline system, relation between stress δ and strain $\in$ is determined by three independent components of the stiffness matrix (also known as Voigt c_{ij} matrix), namely c_{11} (=c_{22}=c_{33}), c_{12} (=c_{13}=c_{23}) and c_{44} (=c_{55}=c_{66}), of the following expression [25]

$$\delta_{ij}=c_{ij}\in_{ij}\ (i,j=1,2\ldots\ldots\ldots.6) \quad (14)$$

The other components of the c_{ij} matrix are zero in the symmetric anisotropy.

Numerical work based on continuum elasticity-based finite element analysis and 'model solid theory' by Van de Walle as reported by Lee et al. [25] will be used to carry out our investigation on the effect of elastic anisotropy on the strain fields and

the band-edge profiles with a view of reducing the strain component (strain minimization) and the magnetic field is set at zero via the input file of nextnano (and also eight-band k·p theory will be used) [40]. In the input file of nextnano, the single band Schrödinger masses were chosen appropriately for a 2D system that is anisotropy. The discretization method for finite differences was used with the electrostatic potential set to zero. Varshni parameters were also switched off and the absolute conduction band as specified in nextnano^3 data base [40] was used.

The modified single band toy model that incorporates quantum confinement induced strain is solved numerically for zinc-blende (zb) InAs QD with spherical shape. No external stress is applied and thus $\varepsilon^0 = 0$ (This shows that even in the complete absence of external strain, i.e. a dilatational strain proportional to the probability density emerges)[11].

Dirichlet boundary conditions are applied during the simulation for electron and hole. We also assume that all the masses for all the principal axes are equal. Valence band warping has also been included in the k.p simulation. The valence band energies for heavy hole (hh), light hole (lh), and split-off holes are calculated by defining an average valence band energy E_{vav}, for all three bands and adding the spin-orbit-splitting (so) energy afterwards.

The spin-orbit-splitting energy is defined together with the k.p parameters. The average valence band energy E_{vav}, is defined on an absolute energy scale and must take into account the valence band offsets which are averaged over the three holes. The energy gap is not temperature dependent and the magnetic field is set to zero. In calculating the energies, the parameters in the input file are chosen such that the strain is set to hydrostatic-strain and the strain is also minimized. The diagonalization for each grid point 6x6 k.p and 8x8 k.p Hamiltonian [11, 26-28] with band edge, non-parabolicities and the density of states were carried out in the simulation using nextnano^3 code [40].

2.2 The Radiative Recombination Rate

For strong size confinement in low dimensional QD that is studied, it has been shown however that the radiactive recombination time can be extended above the 2ns.

In general the effective lifetime τ_{eff} resulting from any measurement is the combined result of bulk lifetime $\tau_b$and surface lifetime τ_s given by [29]

$$\frac{1}{\tau_{eff}} = \frac{1}{\tau_b} + \frac{1}{\tau_s} \quad (15)$$

It is customary to relate nonradiative surface recombination to the surface recombination velocity s and the sample thickness d. For the sample with two surfaces (or interfaces) a and b

$$\frac{1}{\tau_s} = \frac{S_a + S_b}{d} \quad (16)$$

In devices, for which the active thickness is small (like quantum dots, wire, well or even thin film light emitters) surface recombination is the ultimate factor limiting the quantum efficiency τ of the radiative recombination [30, 31].

$$\tau_s = \frac{d}{2\sigma v_{th} N_t} \quad (17)$$

where σ is the capture cross-section of the carriers,v_{th} their thermal velocity and N_t the trap density in the material.

Similarly, bulk lifetime is given by

$$\tau_b = \frac{1}{\sigma v_{th} N_t} \quad (18)$$

From the above considerations it becomes clear that semiconductors with inherently large surface recombination velocity s are not useful as light emitters irrespective of other material parameters [30].

For the radiative, the electron from the conduction band directly combines with the holes in the valence band and releases a photon; and the emitted photon has energy similar to the band gap and is therefore only weakly absorbed [32],

then

$$\tau_{radiative} = \frac{\tau_n \tau_p}{\tau_n + \tau_p} \quad (19)$$

where τ_n and τ_p are electron and hole life times given by

$$\tau_n = (\alpha p_0)^{-1} \quad (20a)$$

$$\tau_p = (\alpha n_0)^{-1} \quad (20b)$$

α is the capture coefficient [32] (and is equal to $2.5x10^{-4}eV/k$). For intrinsic semiconductors $p_0=n_0$, $\tau_n=\tau_p$. There are two ways to lower the surface recombination rate. One is a chemical passivation of the surface [30], while the other involves the formation of a potential barrier that would prevent minority carriers from reaching the surface [29]. Such a potential can be accomplished by making an appropriate heterojunction with low interface recombination rate.

3.0 The Band Structure for Strained InAs QD

The results of our numerical computations are presented in Figures 1 and 2 with Figure 1. Showing the band structure for Strain minimization energy and Figure 2 for hydrostatic strain energy. This we have achieved by setting the Fermi energy

(ε_f) at zero. The conduction band energy lie above the (ε_f) while the valence band energy lie below the (ε_f) level when the strain is minimized but the hydrostatic strain pushes the valence band up to the (ε_f) level as can be seen in Figure 2. As we can see from a direct band gap of InAs QD, there will be a significant charge trapped within the dot so that the recombination of electron hole pairs favours that of type I and type II transitions.

For both cases the bottom of the conduction band is at the same point in k-space as the top of the valence band, so InAs has a direct gap and light can excite electrons across the minimum band gap. The dispersion relation is parabolic at low energies for the bulk material system [33]. This however is not true for the nanostructure that we study as there are no semiconductor with a simple parabolic conduction and valence bands [28].

In the absence of strain effects, the confining potential for an electron (hole) is a square well formed by the difference in the absolute energy of the conduction (valence) band edges [34]. For the conduction band Gamma at E(k=0), the strain minimization energy profiles the depth for the confining potential between 1.2612- 1.4688eV as shown in Figure 1. The two energies component in the conduction band gamma represents the conduction band gamma minimal and maximal and corresponds to the optical transverse (OL) and the longitudinal phonons. The strain induced potentials show wavy variation along this direction for the strain minimization profile and produced unequal values but is non degenerate due to the absence of uniaxial deformation potential at point gamma.

From the experimental observations of Miska et al.[4] under high excitation density, the wetting layer (WL) emission appears at about 1.05eV with a shoulder at 0.98eV between the ground state and the WL. A band gap of 0.54eV was achieved by Miska et al. [4] while in our studies a band gap of 0.75eV was obtained. This value correlates well with the experimental observation of Cheng et al. [35]. Table 1 clearly show the band structure at gamma point obtained by some researchers and the barrier used as strain reduction mechanism.

As stated earlier, the confining potentials for each carrier type is shifted due to the induced strain. This effect is more on the hydrostatic strain energy term pushing the horizontal and vertical confinement on the same level of confining potential (Figure 2). At point L, the confining potential profiles a depth between 1.3232-1.5000eV which is in agreement with the values of 1.4900-1.5200 reported on ref.11, also Cusack et al. [39] obtained a value of 1.5200eV due to the comprehensive strain on the barrier that shift the conduction band slightly above the unstrained GaAs. At point X the hydrostatic strain splits the conduction bands with an offset of 0.9648eV; this observation was also reported in ref. 37. The band structure at these points was used for the computation of the radiative recombination rate.

4.0 Result of the Radiative Recombination Rate Computed.

For the radiative, the electron from the conduction band directly combines with the hole in the valence band and releases a photon. The emitted photon has energy similar to the band gap and is therefore only weakly absorbed.

Here we estimate the surface radiatve recombination rate at various thicknesses (d) of specimen (see Figure 3). The thickness was taken from the band structure computed so far (from Figures1and 2). The radiative lifetimes for the barrier and dot computed so far without annealing temperature are displayed (Figure 3). As can be seen the lifetimes for both samples are in the range of 1.61-10.70ns. The decay times are larger than those regularly observed on this system [5, 37-39]. For the dots where electrons and holes are localized, we were able to get a carrier lifetimes between 1.61-2.14ns compare to a value of 1.08ns reported by Pancholi et al. [5]. The longer radiative lifetimes observed (10-10.7ns) is as a result of type-II transitions, i.e., the electron states are confined in the dots while hole states are localized in the GaAs barrier. The result obtained however shows an improvement with the observed lifetimes in type-I and type II heterojunctions as reported [5, 37-39] for the same material system. We were able to overcome the misfit by a reduction on the barrier height and increment on the dot height. This value to the best of our knowledge has not been observed for type I system in InAs/GaAs QD.

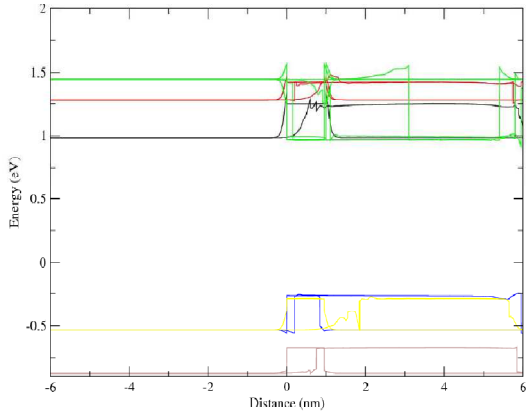

Fig.1: Band structure of GaAs/InAs/GaAs when the Strain energy is minimized (This study). The highest of the valence band energy lies below the Fermi energy level ε_f

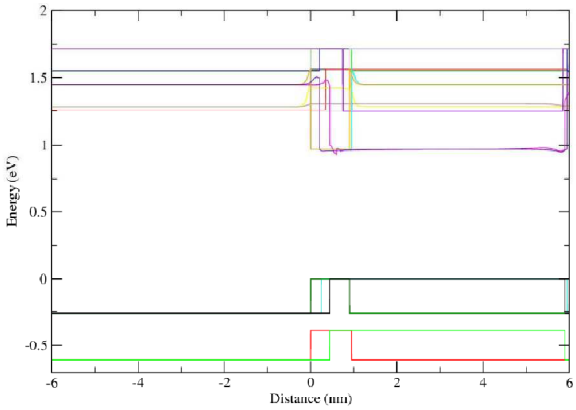

Fig.2: The band structure for GaAs/InAs/GaAs under the influence of hydrostatic strain (This study). The highest of the valence band energy lies at the Fermi energy level ε_f

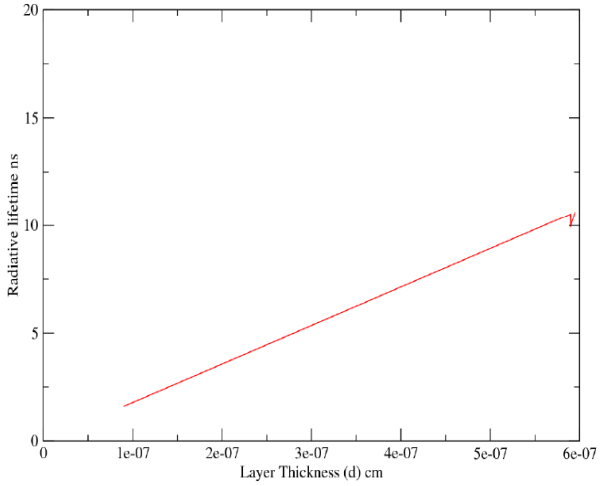

Fig. 3: Radiative recombination rate against the thickness (d) of the specimen. The values used for the computation are obtained from the conduction bands. The thickness between the QDs and barrier are: For the QD, d= $1.2\text{x}10^{-7}$cm, $0.899\text{x}10^{-7}$cm, $0.901\text{x}10^{-7}$, $1.1\text{x}10^{-7}$cm, $0.949\text{x}10^{-7}$cm and for the barrier, $5.901\text{x}10^{-7}$cm, $5.899\text{x}10^{-7}$cm, $6.0\text{x}10^{-7}$cm, $5.951\text{x}10^{-7}$cm (this study).

Table1: Band gap energies for the conduction band obtained.

QD	Barrier	Method used	Band gap energy at Γ (eV)	Conduction band energy (eV)	Unstrained layer	Ref.
InAs	GaAs (110)	Envelope functional Method	0.75	1.50	GaAs	This Study
InAs	GaAs (001)	Effective mass approximation and Finite difference method	0.70	1.52	GaAs	[11]
InGaAs	InP (100)	Experiment	0.75	1.40	InP	[36]
InAs	InP(113)B	Experiment	0.54	1.05	InP	[4]
InAs	GaAs	Envelope functional Method	-	1.52	GaAs	[35]

5.0 Conclusions

Naturally, the band structure of InAs is of type I with the electrons and holes confined in the InAs QDs. This implies that much charge is trapped within the dot for possible applications for photovoltaic energy conversions. This means low quantum efficiency for collection of light generated carriers with the relatively short recombination lifetimes (<2ns) found on this system [5]. The energy levels found on the valence states of this system act as a very efficient ladder for energy loss from the holes and consequently lowering the possible output voltage. With this therefore the quantum efficiency for this system must be increased. This we were able to achieve by extending the recombination lifetimes in InAs type I system to a value of (2.14ns) and the type II system to 10.7ns as against the reported value of less than 2ns and 4ns respectively [5]. This improvement however will help in improving the quantum efficiency of type I system. This we have achieved by ensuring a high carrier mobility and low probability of non-radiative recombination events in the QD structure by lowering the height of the barrier; thereby increasing the confinement and transition energies.

6.0 Acknowledgments

We would like to acknowledge the support from Dr. Stefan Birner for providing us with nextnano^3 code with licence no. 3FC83A37A for our numerical computation.

7.0 References

[1] E-S. Hasaneen, E. Heller, R. Bansal, W. Huang,andF.Jain, Solid-State Electronics 48,(2004) 2055.
[2] A.A. Lagatsky, C.G. Leburn, C.T.A. Brown, W. Sibbett, S.A. Zolotovskaya, and E.U. Rafailov, Progress in Quantum Electronics 34, (2010) 1.
[3] P. Martyniuk, andA. Rogalski, Progress in Quantum Electronics 32, (2008) 89.
[4] P. Miska, J. Even, C. Paranthoen, O. Dehaese, H. Folliot, S. Loualiche, M. Senes, and X. Marie,Physica E 17 (2003) 56.
[5] A. Pancholi, S.P. Bremner, J. Boyle, V.G. Stoleru, and C.B. Honsberg, SolarEnergy Materials and Solar cells 94 (2010) 1025.
[6] R. Enzmann, B. Mario,B. Daniela,H. NÖrman, B. Gerhard, M. Ralf, F. Jonathan and A. Markus-Christian, Journal of Crystal Growth 312, (2010) 2300.
[7] G. Rezaei, M.R.K. Vahdani, and B. Vaseghi,Current applied Phys. xxx (2010) 1.
[8] G. Rezaei, Z. Mousazadeh, and B. Vaseghi, Physica E 42, (2010) 1477.
[9] L. Cui-Hong, and X. Bai-Ru, Physics Letters A 372, (2008) 888.
[10] Z. Zhi-Hai, G. Kang-Xian, C. Bin, W. Rui-Zhen, K. Min-Wu, andS. Shuai, Superlattices and Microstructures 47, (2010) 325.
[11] X. Zhang, M. Gharbi, P. Sharma, and T.H. Johnson,international journal of solidstates and structures 46 (2009) 3810.
[12] I. Filikhin, V.M. Suslov, M.H. Wu, and B. Vlahovic, Physica E 40 (2008) 715.
[13] W.L. Sarney, L. Salamanca-Riba, J.D. Bruno, and R.L. Tober., Solid-StateElectronics 46 (2002) 1643.
[14] A. Bouazra, S. Abdi-Ben, A. Nasrallah, and M.S. Poncet, Superlattices andMicrostructures 48 (2010) 1.
[15] A.W. Lam, and T.Y. Ng, Computational materials science 49 (2010) S54.
[16] C. Youping, D.L. James, and E. Azim, International Journal of EngineeringScience 41 (2003) 61.
[17] R. Ferreira, O. Verzelen, andG. Bastard, Physica E 21, (2004) 164.
[18] R. Heitz, M. Veit, N. N. Ledentsov, A. Hoffmann, and D. Bimberg, V. M.Ustinov, P. S. Kopev, and Zh. I. Alferov, Physical Review B 56, (1997) 10435
[19] Weidong Yang, Roger R. Lowe-Webb, Hao Lee, and Peter C. Sercel, PhysicalReview B 56, (1997) 13314.
[20] R. Heitz, M. Veit, A. Kalburge, Q. Xie, M. Grundmann, P. Chen, N.N.Ledentsov, A. Hoffmann, A. Madhukar, D. Bimberg, V.M. Ustinov, P.S. Kopev, Zh.I. Alferov, Physica E 2, (1998) 578.
[21] L.P. Janet, Physical Review B 49, (1994) 11272.
[22] Philippe Guyot-Sionnest, Moonsub Shim, Chris Matranga, and Margaret Hines,Physical Review B 60, (1999) R2181.
[23] V.I. Ivan, E.K. Igor, G.D. Valentin, V.N. Selvakumar, L. Jeong-Sik, R. Hong-Wen, S. Shigeo, and M. Yasuaki, Physical Review B 63, (2001) 075316-1.
[24] L. Bin, G. Kang-Xian, Z. Chao-Jin, and Z. Yun-Bao, Physics Letters A 367, (2007) 493.
[25] W. Lee, J-M. Myoung, Y-H. Yoo, and H. Shin, Solid State Communications 132, (2004) 135.
[26] P.C. Sercel, Physical Rev. letters 83, (1999) 2394.
[27] P.C. Sercel, and K.J. Vahala, Physical review B, 42, (1990) 3690.
[28] A.L. Efros, and M. Rosen, Physical Rev. B 58, (1998) 7120.
[29] J.S. Rimmer, I.D. Hawkins, and B.J. Hamilton, Appl. Phys. 70**,** (1991) 5404

[30] J.M. Langeri, and W. Walukiewicz, 18th ICDS, Sendai, July 24-28, (1995)
[31] V.K. Khanna, Eur. J. Phys. 25**,** (2004) 221.
[32] I.N. Volovichev, G.N. Logvinov, O.Y. Titov, and G.Y. Gurevich, J. Appl.Phys.95, (2004) 44
[33] J.H. Davies, Cambridge University press (1998).
[34] M.A. Cusack, P.R. Briddon, and M. Jaros, Physica B 53, (1998) 10.
[35] K.Y. Cheng, A.Y. Cho, S.B. Christman, T.P. Pearsall, and J.E. Rowe, Appl. Phys. Lett. 40, (1982) 423
[36] F.J. Towner, Journal of vacuum science and tech. B 14, (1995) 2315.
[37] H. Yu, S. Lycett, C. Roberts and R. Murray, Applied Physics letters 69, (1996) 4087.
[38] Y.C. Zhang, A. Pancholi, and V.G. Stoleru, Applied Physics letters, 90, (2007) 183104.
[39] M.A. Cusack, P.R. Briddon, and M. Jaros, Physica B 53, (1998) 10.
[40] A. Trellakis, T. Zibold, T. Andlauer, S. Birner, R. K. Smith, R. Morschl, and P.Vogl, J. Comput. Electron. 5, (2006) 285. For the nextnano3 code, see*http://www.nextnano.de*.